Research article

Carbon Future

Cu-doped $CeMnO_2$-supported Pt catalysts with high activity at industrial operating conditions for preferential CO oxidation in H_2

Jianlin Cao[1,#], Tao Xing[2,#], Zongzhuang Sun[1], Sheng Wei[1], Jiaqi Wang[1], Lexin Mao[1], Tao Liu[2], Zhi Li[2], Yongxiao Tuo[1], Xin Zhou[4]✉, Hao Yan[1], Yibin Liu[1], Xiang Feng[1]✉, Chaohe Yang[1], and De Chen[3]✉

[1] *State Key Laboratory of Heavy Oil Processing, China University of Petroleum (East China), Qingdao 266000, China*
[2] *Shandong Energy Group Co., Ltd., Jinan 250000, China*
[3] *Department of Chemical Engineering, Norwegian University of Science and Technology, Trondheim 7491, Norway*
[4] *Department of Chemistry and Chemical Engineering, Ocean University of China, Qingdao 266100, China*

Cite This: *Carbon Future* **2025**, *2*, 9200038

Read Online

ABSTRACT: Developing efficient, stable, and inexpensive catalysts for the preferential CO oxidation in H_2 (CO-PROX) over a wide temperature range in the presence of CO_2 and H_2O is indispensable for the hydrogen purification process. Herein, CuO was introduced to the $CeMnO_2$-supported Pt catalyst to modulate the oxygen activation capacity and provide the available number of active sites in CO-PROX. One part of the CuO species doped into CeO_2 strongly interacts with Ce, thus enhancing the oxygen transfer capacity of the catalyst. The other part of CuO species located on the surface of the catalyst provides extra Cu^+ sites available for low-temperature CO adsorption. This synergistic interaction with Pt sites further enhances CO and O_2 activation, broadening the temperature window of high activity. The optimal Pt-10CuO/$CeMnO_2$ catalyst exhibits complete CO conversion (CO/O_2 ratio of 1:1) within the practical temperature range of 130–190 °C, even in the presence of CO_2 and H_2O, and remains stable at 150 °C for 76 h testing without any deactivation. This work will give a novel approach for the design of highly efficient inexpensive catalysts for industrial preferential oxidation of CO in H_2, especially in the presence of CO_2 and H_2O.

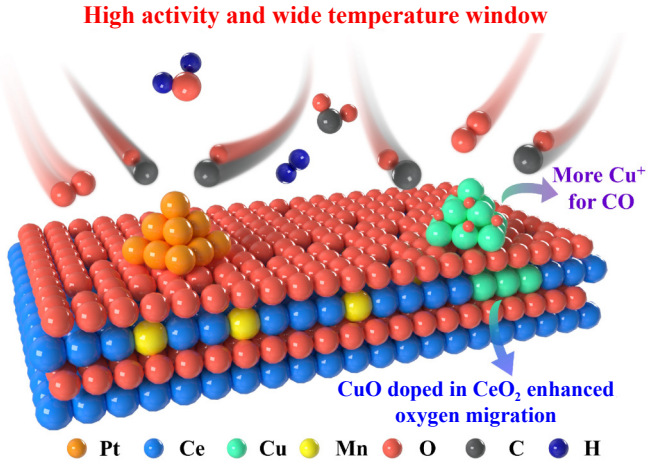

KEYWORDS: preferential oxidation of CO, Cu catalyst, wide temperature window, realistic condition, dual active sites

1 Introduction

Hydrogen, exceeding 94 million tons of production per year, is predominantly obtained through steam reforming of natural gas or coal[1, 2]. Such hydrogen resource contains about 1%–3% CO that must be removed to avoid the severe side-effect in many hydrogen application processes, including proton-exchange membrane fuel cells (PEMFCs) and ammonia synthesis[3–7]. Among the various methods of hydrogen purification, the preferential oxidation of CO (CO-PROX) is acknowledged as the straightforward approach for achieving acceptable CO concentrations (below 50 ppm)[8,9].

Due to the high temperature of outlet H_2 in industrial methanol reforming reaction (ca. 200 °C) and the huge adiabatic temperature rise caused by the oxidation of CO, the efficient CO-PROX catalyst must exhibit high activity and selectivity for CO oxidation at the wide operating temperature range (100–200 °C)[10–12]. In addition, considering the typical composition of the industrial feed gas which often includes large amount of CO_2 and H_2O, the catalysts must exhibit robust tolerance towards these two components. Noble-metal catalysts, particularly Pt-based catalyst, have been identified as candidates for effective CO-PROX reactions. However, at low temperatures around 110 °C, the activity of Pt catalysts is generally low[13–15]. In order to enhance the activity of Pt catalyst to broaden the reaction temperature, metal oxides (e.g., CeO_2 and ZrO_2) with a certain redox capacity have been selected as support for Pt catalysts. Nevertheless, the catalysts with high catalytic performance often

Received: November 25, 2024; **Revised:** January 25, 2025
Accepted: February 4, 2025

✉Address correspondence to Xiang Feng, xiangfeng@upc.edu.cn; Xin Zhou, xinzhou@ouc.edu.cn; De Chen, de.chen@ntnu.no
#Jianlin Cao and Tao Xing contributed equally to this work.

https://doi.org/10.26599/CF.2025.9200038

require a high content of Pt (1.5 wt.%–10 wt.%)[16, 17], which will drive up the cost of the catalyst dramatically. Therefore, the transition bimetallic oxide catalyst CuO-CeO_2, which has high catalytic activity with low cost and easy availability, can be introduced as a modifier to Pt-based catalysts to reduce the cost[18–20]. The high catalytic activity is mainly attributed to the synergistic effect between CuO and Ce, and the remarkable oxygen release capacity of CeO_2. This process can be further enhanced by doping other cations[1, 3, 20] (e.g., Mn and La) into the lattice of Ce. In addition, CO can also react with the hydroxyl groups adsorbed on CeO_2 to form carboxyl intermediates, which will accelerate the activation of CO[21, 22]. Conversely, the feedstock contains a large amount of CO_2 and H_2O, which may compete with the reactants for adsorption on the surface of the catalyst[23–26]. This competition will hinder the reaction process. Nevertheless, the incorporation of transition metals like Cu and Ce into Pt catalysts can mitigate this competitive adsorption phenomenon. Thus, the research on Pt-based catalysts in the presence of H_2O and CO_2 is still lacking and highly desired.

On Pt-based catalyst, Cu species were normally doped in the lattice of reducible MO_x in order to modulate the electronic structure of Pt and MO_x. For instance, the incorporation of metal oxides (e.g., Cu and Ni) to induce an electron deficient state in Pt has been demonstrated to attenuate CO adsorption[14, 27, 28], while the introduced reducible MO_x could also enhance the ability of oxygen migration[29, 30]. It is reported that PtCu inter-metallic compounds supported on silica catalysts (IMCs) are capable of acting as effective catalysts for CO-PROX at 100–180 °C under the effect of cooperative redox enhancement[13, 31, 32]. In addition, numerous experiments have demonstrated that the interaction between Pt and CuO can reduce the average diameter of CuO particles, promote the production of oxygen vacancies, and enhance oxygen mobility, thus accelerating the reaction. The transition metal ions (e.g., Cu and Ni) doped into the lattice of MO_x make it difficult to achieve highly active CO-PROX in the wide temperature region because of the difficulty in providing Cu^+ sites for CO adsorption. Hence, there is great need to judiciously harness the oxygen activation capability and CO adsorption ability of CuO, facilitating synergistic interaction with Pt and showing excellent catalytic activity over a wide temperature range in the presence of CO_2 and H_2O.

In this work, we prepared Pt-CuO/$CeMnO_2$ tetrameric catalysts using a co-precipitation method combined with a modified impregnation method, aiming to design catalysts capable of achieving efficient and selective CO removal under realistic industrial conditions. The Pt-10CuO/$CeMnO_2$ catalyst exhibited exceptional catalytic performance and stability at the wide working temperature range (130–190 °C). Through multi-characterizations (e.g., H_2-temperature programmed reduction (H_2-TPR), X-ray photoelectron spectroscopy (XPS), and *in-situ* diffuse reflectance infrared fourier transform (DRIFT)), it is found that CuO has two important roles for CO-PROX reaction. One part of the CuO species doped into the CeO_2 lattice provides a chemical interface between CuO and CeO_2 which accelerates the activation of oxygen species. Additionally, the other part of the CuO species located on the surface of catalyst provides Cu^+ for the adsorption of CO. Due to the coupling of these two functions by CuO, the wide activity temperature range (130–190 °C) of the catalyst in the presence of H_2O and CO_2 is obtained. The results provide guiding significance to regulate the catalyst microenvironment to enhance the preferential oxidation of CO in H_2 in the presence of H_2O and CO_2.

2 Experimental

2.1 Chemicals

Cerium nitrate hexahydrate ($Ce(NO_3)_3{\cdot}6H_2O$, 99.9%) and chloroplatinic acid ($H_2PtCl_6{\cdot}6H_2O$, 99.9%) were purchased from Maclin. Sodium hydroxide (NaOH, 96.0%) was got from Alfa Aesar, while copper(II) acetate monohydrate ($Cu(CH_3COO)_2H_2O$, 99.9%) and manganese nitrate solution ($Mn(NO_3)_2$, 50 wt.% in H_2O) were purchased from Aladdin.

2.2 Material preparation

2.2.1 *Preparation of CuO/$CeMnO_2$*

CuO/$CeMnO_2$ was prepared via the co-precipitation method. Firstly, 10.19 mL of 1 M cerium nitrate aqueous solution was added to 50 mL of deionized water at 30 °C. After stirring for 10 min, a certain amount of copper acetate monohydrate and 0.2 g of manganese nitrate solution were added into the solution. After stirring vigorously for 20 min, 1 M NaOH solution was added to adjust the pH of the solution to 9. The above solution was stirred at 60 °C. Finally, the precipitate was washed with 3 L of deionized water, and then dried overnight at 80 °C and calcination in a muffle furnace at 500 °C for 3 h. Different CuO loadings were obtained by adjusting the quantities of the copper acetate solution precursor.

2.2.2 *Preparation of Pt-CuO/$CeMnO_2$*

Pt-CuO/$CeMnO_2$ was prepared by incipient-wetness impregnation method[28]. Firstly, 1.5 g of CuO/$CeMnO_2$ was initially suspended in 80 mL deionized water, while maintaining constant stirring at a temperature of 80 °C. The appropriate amount of H_2PtCl_6 aqueous solution was gradually introduced into the aforementioned mixture while continuous stirring for approximately 7 h until it achieved a consistent colloid-like state. Subsequently, it was aged at 80 °C for 12 h.

2.3 Catalytic evaluation

The evaluation of the catalytic in the CO-PROX reaction was conducted using a fixed-bed reactor. Firstly, 300 mg of catalyst was placed into the quartz tube reactor and subjected to a 2 h reduction with a mixture of 10% H_2/N_2 (120 mL·min^{-1}) at 200 °C. Then, the catalyst was cooled to 30 °C and the reaction mixture gas (H_2:CO:O_2:H_2O:CO_2:N_2 = 60:1:1:17:20:1) was introduced with a flow rate of 100 mL·min^{-1}. The catalytic activity testing was conducted within a temperature range of 90–200 °C, with the interval of 20 °C. An Agilent 8890 gas chromatograph which equipped with flamed ionization detector (FID) and thermal conductivity detector (TCD) was used for online product analysis. The CO conversion and the CO_2 selectivity were calculated as follows (Eqs. (1) and (2))

$$\text{The conversion of CO} = \frac{[\text{CO}]_{\text{in}} - [\text{CO}]_{\text{out}}}{[\text{CO}]_{\text{in}}} \times 100\% \quad (1)$$

$$\text{The selectivity of CO}_2 = 0.5 \times \frac{[\text{CO}]_{\text{in}} - [\text{CO}]_{\text{out}}}{[\text{O}_2]_{\text{in}} - [\text{O}_2]_{\text{out}}} \times 100\% \quad (2)$$

where $[CO]_{in}$ and $[O_2]_{in}$ represent the mole content of CO and O_2 in the reactant gas, respectively, and $[CO]_{out}$ and $[O_2]_{out}$ are the mole content in the product gas.

2.4 Characterizations

The X-ray diffraction patterns of the catalysts were collected by a Panalytic X'pert PRO MPD diffractometer which equipped with a Cu-Kα radiation. The element loadings of catalysts were ascertained via inductively coupled plasma-atomic emission spectroscopy (ICP-AES) (Agilent 7700 system). The N_2 adsorption–desorption isotherms of the prepared catalysts were determined using a Micromeritics ASAP 2460 instrument. A JEOL JSM-2100F microscope was used to capture the high-resolution transmission electron microscopy (HRTEM) images of catalysts. The XPS analysis of catalysts were measured by a PHI 5000 Versaprobe II system. The H_2-TPR analysis was conducted by a Micromeritics Auto Chem II 2920, which equipped with a thermal conductivity detector (TCD) detector.

The *in-situ* DRIFT spectra was collected by a Nicolet S10 which equipped with mercury cadmium telluride (MCT) detector cooled by liquid nitrogen. For the elimination of the impurities adsorbed on surface, the sample (about 200 mg) was initially subjected to treatment in Ar atmosphere with the flow rate of 50 mL·min^{-1}. Subsequently, the background was obtained to facilitate spectral correction, following the cooling of the sample to 30 °C. Subsequently, the mixture gas was introduced into the chamber (the flow rate was 15 mL·min^{-1}) and maintained at a temperature of 80 °C. The spectra were acquired under different reaction conditions, with 32 scans accumulated at a resolution of 1 cm^{-1}.

3 Results and discussion

3.1 Physical structure of different Pt-CuO/CeMnO$_2$ catalysts

By using the precipitation method, the CuO/CeMnO$_2$ catalyst was synthesized, followed by the deposition of Pt onto CuO/CeMnO$_2$ using a modified co-impregnation approach. **Fig. 1a** shows the structure model of the catalyst before and after the introduction of CuO. The X-ray diffraction (XRD) patterns of Pt-CuO/CeMnO$_2$ are shown in Fig. 1b. The results indicate that the predominant structure of the catalysts consists of a face-centered cubic fluorite structure CeO_2 (JCPDS No. 081-0792) in combination with a monoclinic structure CuO (JCPDS No. 080-0076)[33], and the complete JCPDS cards about CuO and CeO_2 are shown in Supplementary Fig. S2. The distinct peaks at 28.4°, 33.2°, 47.3°, and 56.3° correspond to the crystallographic planes (111), (200), (220), and (311), respectively, within the structure of CeO_2 is face-centered cubic. The characteristic peaks at 35.6° and 38.8° represent the (002) and (111) crystal faces of the monoclinic CuO, respectively[31, 34]. The diameters of Mn ions (Mn^{2+}: 0.67 Å, Mn^{3+}: 0.62 Å, and Mn^{4+}: 0.56 Å) are much smaller than the radii of Ce ions (Ce^{3+}: 1.1 Å and Ce^{4+}: 1.01 Å)[35]. Consequently, manganese ions possess the ability to incorporate into the lattice of CeO_2, leading the formation of CeMn solid solutions. Therefore, the XRD spectra do not exhibit the characteristic peaks belonging to Mn oxides, indicating that the Mn species were doped into CeO_2, resulting in a robust interaction between the MnCe solid solution and cerium[30, 36], which is beneficial to increase the dispersion of CeO_2, strengthening the degree of reduction of CeO_2 and accelerating the formation of O_{vac}. In addition, there is no distinct diffraction peaks corresponding to Pt species in the XRD patterns of the catalysts, indicating the high dispersion of Pt on catalyst. The exact contents of Pt and CuO determined by ICP and the porosity properties of catalysts are shown in Supplementary Table S1. The loadings were 0.38% for Pt and ranged from 5.1% to 34.2% for CuO. As shown in Supplementary Table S1, the pore size of the catalysts increased from 4.8 to 6.1 nm with the increase of the content of CuO, which may be caused by the accumulation of excess CuO particles. Similarly, in Fig. 1c, all catalysts exhibited H-3 type hysteresis back loops, indicating the presence of pore channels in the catalysts generated by particle accumulation.

The microstructure of catalyst and the corresponding effects of CuO introduction were further characterized by TEM. A large number of small particles with diameter of about 6.36 nm (Supplementary Fig. S1a) stacked together and formed pore channels, which is shown in Fig. 1d. There is an abundant contact interface between CuO and CeO_2 in the HRTEM images and the lattice spacing of CeO_2 is 0.315 nm, which is smaller than 0.323 nm (Supplementary Fig. S3), indicating that part of CuO was doped into CeO_2[37] (Figs. 1d and 1e), and the synergistic interactions existed in the interface between CeO_2 and CuO, which will promote the cooperative redox enhancement effect. Upon the introduction of CuO, the lattice spacing of the CeO_2 (111) crystal plane reduces to approximately 0.315 nm, a value smaller than that of CeO_2 (0.32 nm), further confirming the formation of a ternary oxide solid-phase mixture of CuO/CeMnO$_2$. As shown in Figs. 1d and 1e, TEM-energy dispersive X-ray spectroscopy (EDS) mapping of catalyst within a selected region illustrated that the distribution of Ce, Cu, and Pt elements is homogeneous in the catalyst.

3.2 Enhanced catalytic performance of the Pt-CuO/CeMnO$_2$ catalysts

The Pt/CeMnO$_2$ and 10CuO/CeMnO$_2$ catalysts performed poorly in the CO-PROX reaction under practical conditions (60% H_2, 1% CO, 1% O_2, 20% CO_2, 17% H_2O, and 1% N_2), failing to achieve 100% CO conversion in the temperature range of 90–200 °C, as shown in **Fig. 2a**. However, with the presence of both Pt and CuO, the reactivity of the catalyst is significantly improved, and the complete removal of CO can be achieved at 130–190 °C when the space velocity is 20,000 mL·h^{-1}·g$_{cat}^{-1}$. The significant performance enhancement emphasizes the cooperative interactions between CuO and Pt. As shown in Fig. 2b, the conversion of O_2 increases with the increase of temperature and reaches 100% conversion after 130 °C. Besides, the introduction of CuO in the system enhances the conversion of O_2 at low temperatures (90–130 °C), which provides a prerequisite for the broadening of the temperature windows. The CO_2 selectivity curve of the catalyst can be observed in Fig. 2c. The selectivity of the catalyst decreases with the increase of temperature, resulting in the oxidation of H_2 with O_2 at high temperatures, due to a decrease in selectivity due to the reaction of O_2 with H_2. Thus, it is difficult to achieve both the highest CO conversion and the highest CO_2 selectivity at real industrial temperature conditions (80–200 °C). However, the negligible loss of H_2 pales in comparison to the severe toxic impact of residual CO on the Pt electrode within the PEMFC cell. Therefore, Pt-CuO/CeMnO$_2$ catalyst was still considered as an effective catalyst capable of catalyzing the CO-PROX reaction with the presence of H_2O and CO_2.

The effect of different CuO loadings on the activity of catalysts is shown in **Fig. 3**. We found that the content of CuO has an optimal ratio which can efficiently catalyze the CO-PROX reaction. When the content of CuO is 10%, the catalyst has the widest efficient range of complete CO conversion (130–190 °C) in the presence of

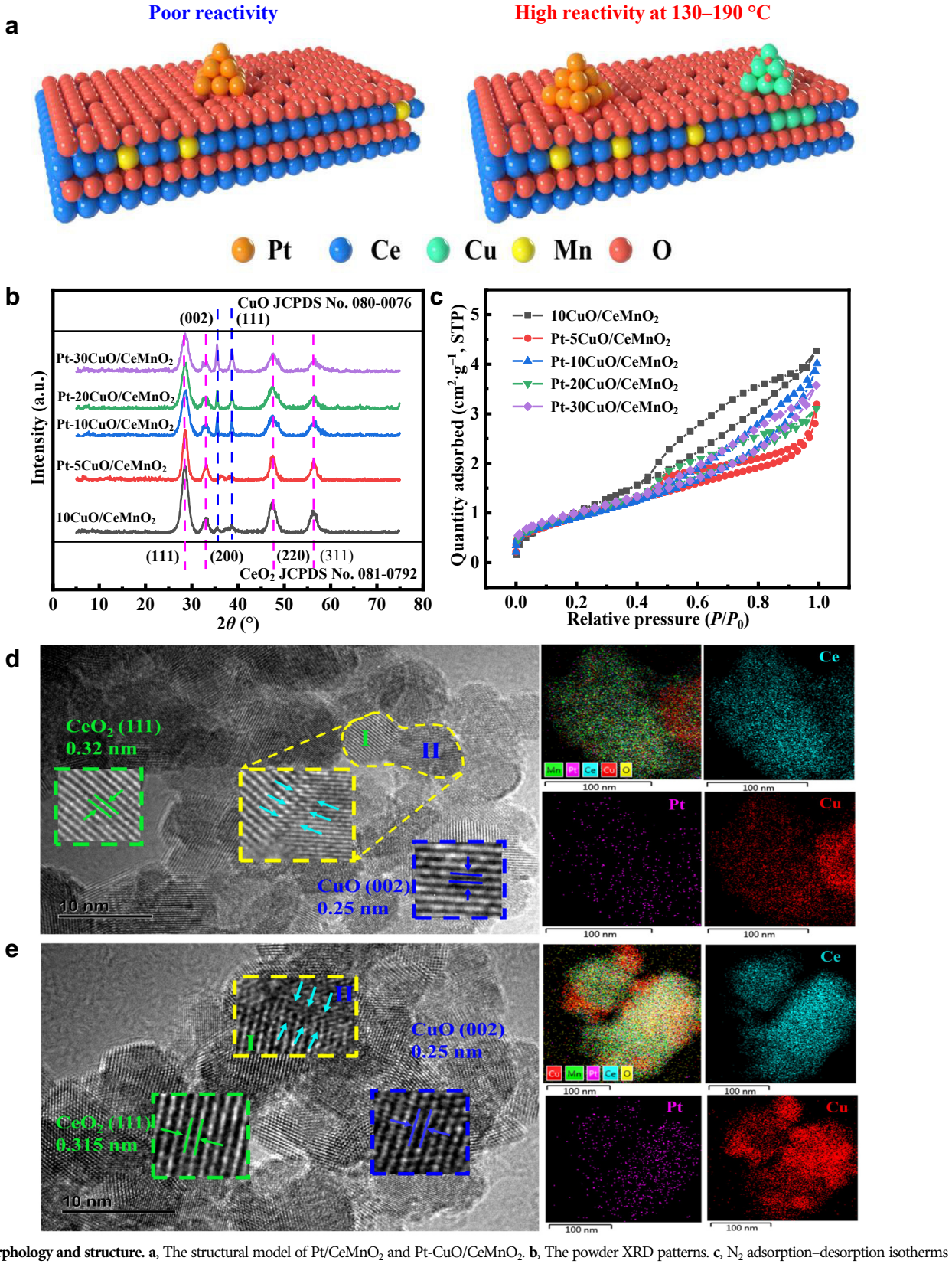

Fig. 1. Morphology and structure. a, The structural model of Pt/$CeMnO_2$ and Pt-CuO/$CeMnO_2$. **b**, The powder XRD patterns. **c**, N_2 adsorption–desorption isotherms for various catalysts. **d**, TEM images of Pt-5CuO-$CeMnO_2$ catalyst. **e**, TEM images of Pt-10CuO/$CeMnO_2$ catalyst.

H_2O and CO_2. Subsequently, the comparison of the CO-PROX reaction activity of different catalysts reported in the literature can be observed in Fig. 2d and Supplementary Table S2. The Pt-10CuO/$CeMnO_2$ catalyst has a wider CO complete conversion temperature window (130–190 °C) than the catalysts reported in literatures under the same conditions.

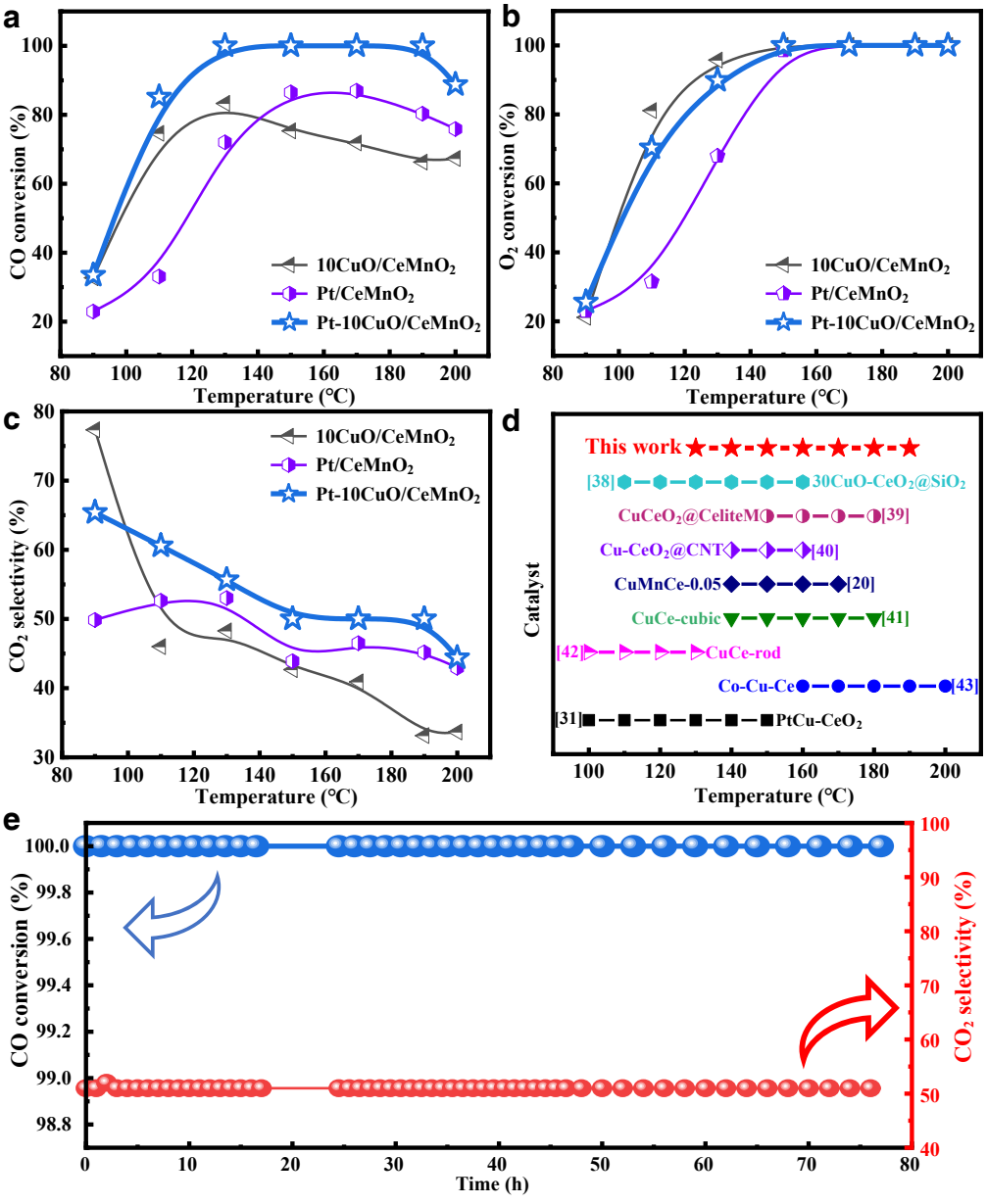

Fig. 2. The catalytic activities. a–c, The CO conversion (a), the O_2 conversion (b), and the CO_2 selectivity (c) for CO-PROX reaction. **d**, The comparation of the temperature window (the CO conversion is 100%) in this work with that of CuO_x-CeO_2 based catalysts reported in literatures. **e**, The stability at 150 °C (the space velocity is 20,000 $mL \cdot h^{-1} \cdot g_{cat}^{-1}$) for Pt-10CuO/$CeMnO_2$. Reaction conditions: 60% H_2 + 1% CO + 1% O_2 + 20% CO_2 + 17% H_2O + 1% N_2[20,31,38–43].

3.3 The chemical structure of different Pt-CuO/$CeMnO_2$ catalysts

Figs. 4a–4d exhibit the results of XPS spectra of different catalysts. The results of Ce 3d curves with different catalysts are shown in Fig. 4a. The two spin-orbital multiplets corresponding to $3d_{3/2}$ and $3d_{5/2}$ are denoted as $u(u - u''')$ and $v(v - v''')$, respectively. The peaks denoted as u' (903.1–903.8 eV) and v' (885.0–885.7 eV) are attributed to Ce^{3+}, while the other six peaks were assigned to the Ce^{4+} [44–46]. The presence of Ce^{3+} in the result of XPS identified the reduction of Ce^{4+} and the formation of oxygen vacancies[47]. As the relative content of Ce^{3+} increases, the rate of oxygen migration is elevated, and consequently the performance of CO-PROX is enhanced. The content of Ce^{3+} can be calculated from the peak area of Ce^{3+} to the total peak area of Ce^{n+}. As shown in Table 1, the rise in surface Ce^{3+} content and the augmentation of oxygen vacancies correlate with the appropriate increase of CuO loading. The reason is that CuO tends to aggregate on the surface of CeO_2 with the increase of CuO content, covering a certain amount of Ce^{3+} sites. This relationship is intrinsically linked to the cooperative redox enhancement effect originating from CuO and CeO_2. Oxygen vacancies are considered to be mobile reactive sites in the CO-PROX reaction, which can participate in the reaction by activating and dissociating O_2, and the abundance of oxygen vacancies will enhance the reactivity of surface oxygen in the process of the CO-PROX reaction[41,48].

As shown in Fig. 4b, the peaks of Pt $4d_{3/2}$ and Pt $4d_{5/2}$ are situated at 315.9 and 332.1 eV, respectively, aligning with the characteristic values for Pt^0 [49,50]. With the introduction of Cu into the catalyst, a significant negative shift for the binding energy of the peaks was observed, which effect between Pt and Cu. Due to the fact that the

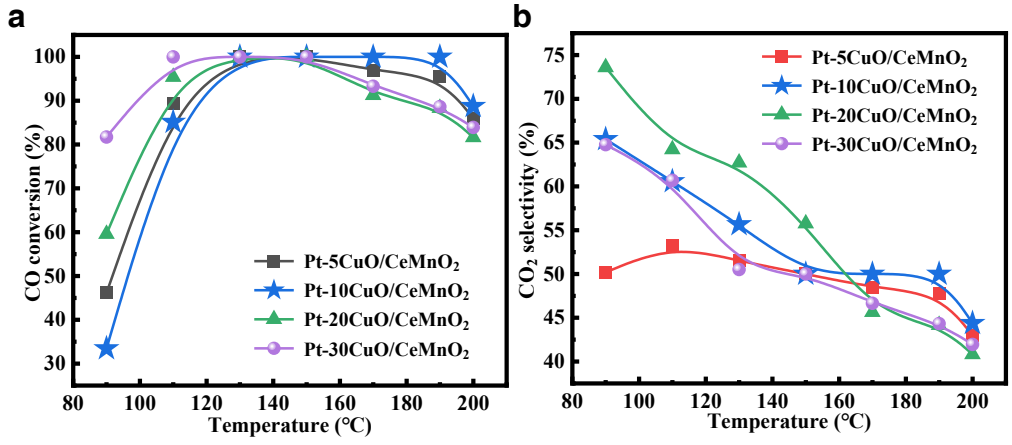

Fig. 3. The catalytic activities. a, b, The CO conversion (a) and the CO_2 selectivity (b) for CO-PROX for different catalysts. Reaction conditions: 60% H_2 + 1% CO + 1% O_2 + 20% CO_2 + 17% H_2O + 1% N_2.

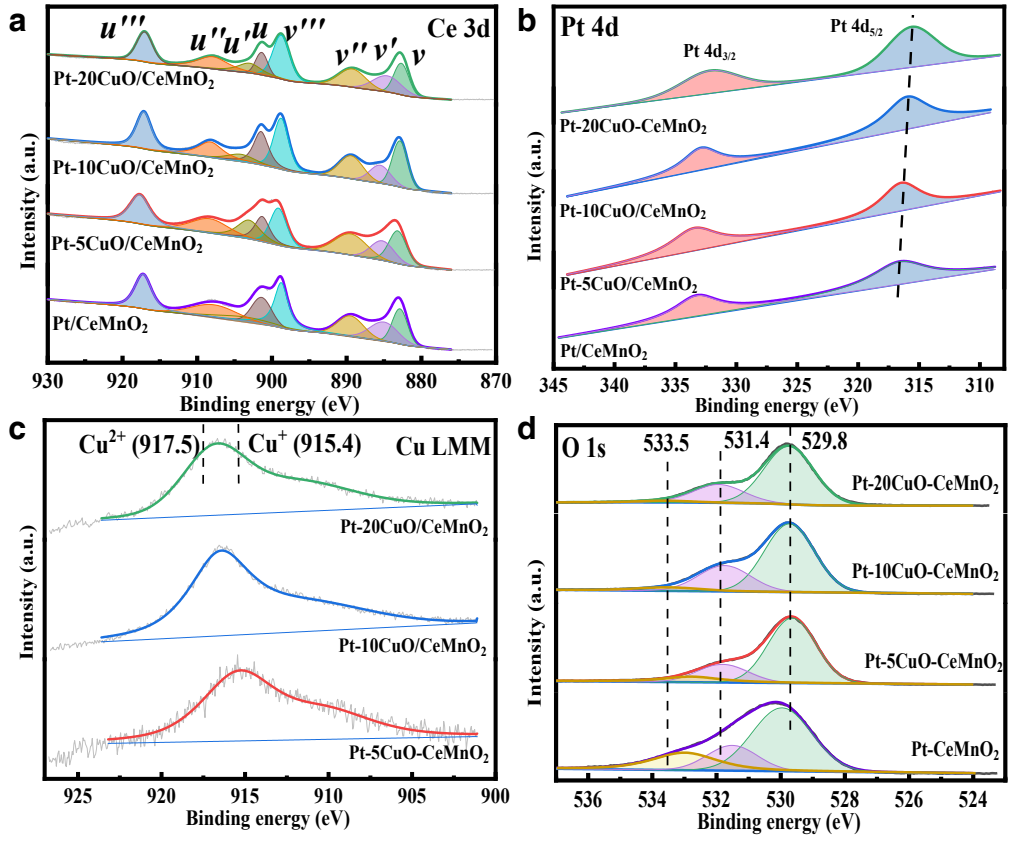

Fig. 4. The electronic properties. a–d, The XPS spectra of Ce 3d (a), Pt 4d (b), Cu LMM (c), and O 1s (d).

Table 1 XPS results for various catalysts

Sample	Ce^{3+} (%)[a]	O_{vac} (%)	I_{sat}/I_{mp}[a]	Cu_{LMM} KE (eV)
$Pt/CeMnO_2$	9.46	18.43	—	—
$Pt\text{-}5CuO/CeMnO_2$	11.63	20.47	0.41	915.9
$Pt\text{-}10CuO/CeMnO_2$	15.1	26.81	0.41	916.1
$Pt\text{-}20CuO/CeMnO_2$	13.01	24.73	0.36	916.65

[a]Calculated from XPS measurements.

Fermi energy level of Pt site is lower than that of Cu, electron transfer from Cu to Pt occurs during hybridization between neighboring atoms, thus leading to the increase in the electron density on the Pt surface[7, 41, 51].

The XPS spectra of Cu 2p are shown in Supplementary Fig. S6. The XPS spectra of Cu 2p revealed a composition of two peaks, specifically Cu $2p_{3/2}$ and Cu $2p_{1/2}$, respectively. The peak of Cu $2p_{3/2}$ within the range of 933.0–933.8 eV, along with the presence of a strong shake-up satellite peak, represents distinctive attributes of Cu^{2+} species. The two valence states of Cu arise due to the robust interaction between Ce oxides and Cu during calcination[52–54]. According to the literatures, the reduction degree of copper can be estimated by the I_{sat}/I_{mp} ratio, which can be calculated from intensity ratio of shake-up satellite peaks to main peaks, as indicated by the Cu $2p_{3/2}$ peaks[55, 56]. As shown in Table 1, after the incorporation of CuO, the catalysts contained significant amounts of Cu^+, indicating the presence of reducible copper species that serve as CO adsorption sites, which are crucial for enhancing the performance of CO-PROX. In order to provide a comprehensive elucidation of the oxidation states of Cu species, the Auger LMM line results of Cu are presented in Fig. 4c. The binding energy of Cu $2p_{3/2}$ and the kinetic energy of Cu LMM Auger electrons are listed in Table 1. The kinetic energy of metallic Cu species in Cu LMM Auger electrons typically exceeds 918 eV. The significantly diminishing of Cu LMM Auger electrons suggested a prevalent presence of copper in the Cu^+ form within the catalysts. With this as a benchmark, we can more accurately obtain the Cu^+ content in the catalyst: Pt-10CuO/$CeMnO_2$ ≈ Pt-20CuO/$CeMnO_2$ > Pt-5CuO/$CeMnO_2$.

The O 1s of the catalyst can be observed in Fig. 4d. The peak located at 529–531.0 eV is generally considered as the peak of O_{latt}. The peak located at 531–532 eV is generally considered as the peak of O_{vac}. The peak (533–535 eV) is linked to chemisorbed oxygen (O_{ads}), which includes carbonic acid hydroxyl groups, adsorbed oxygen, and adsorbed water[57, 58]. It is shown in Fig. 4d that the positions of two kind oxygen species peaks shifted to lower binding energies after CuO introduction. This shift can be attributed to electronic interactions between Pt and Cu or Ce. The formation of O_{vac} can be observed on the result of electronic paramagnetic resonance (EPR) (Supplementary Fig. S5), and the catalyst formed a large amount of O_{vac}, which was beneficial to the acceleration of oxygen activation[59, 60].

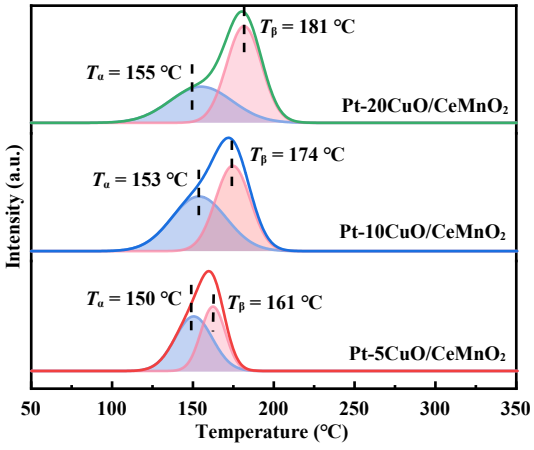

Fig. 5. The H_2-TPR spectra of different catalysts.

To further investigate the valence state of the copper species and the active site in the process of reaction, we performed H_2-TPR and *in-situ* DRIFT characterization on the catalysts. As shown in **Fig. 5**, there are two reduction peaks clearly presented below 250 °C for each catalyst, indicating a two-step surface reduction process for the samples[61]. The low-temperature broad band centered at 110–170 °C (T_α) originates from the highly dispersed CuO_x cluster, a species attributed to the formation of the Cu-[O_x]-Ce structure with strong interactions with Ce. In contrast, the temperature peak located at 170–230 °C (T_β) can be attributed to the reduction of an isolated CuO species, which interacted Ce weakly[62]. In addition, the reduction peak of PtO_x appears around 130 °C, which overlaps with the reduction of the highly dispersed CuO species. Besides, the reduction peak of isolated manganese oxides usually occurs at about 540 °C. However, there is no signal of manganese oxides being found in Fig. 5, which may be due to the doping of manganese into the lattice of CeO_2 and the extremely strong interaction with Ce. The actual hydrogen consumption of the catalyst is shown in Supplementary Table S3. It is noteworthy that the consumption of H_2 is higher than the theoretical values of CuO and Pt measured by ICP. This indicates that in addition to the reduction of the PtO_x and CuO, part of the surface CeO_2 was also reduced, which suggestes that the reduction extent of Ce species and the oxygen transfer capacity of the catalyst are enhanced after the introduction of CuO.

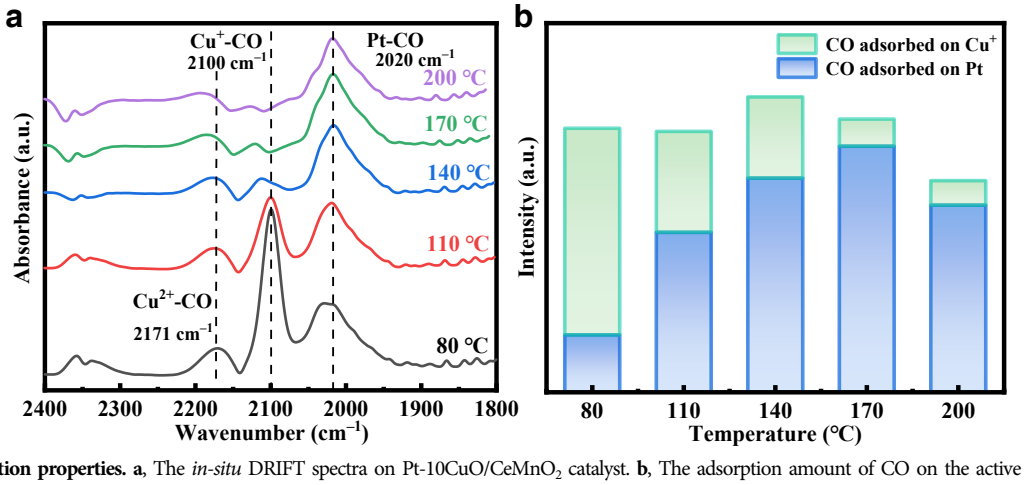

Fig. 6. The adsorption properties. a, The *in-situ* DRIFT spectra on Pt-10CuO/$CeMnO_2$ catalyst. **b**, The adsorption amount of CO on the active site spectra on Pt-10CuO/$CeMnO_2$. The composition of mixture gas used for the DRIFTS test was 1% CO + 1% O_2 + 60% H_2 + 20% CO_2 + 3% H_2O, balanced in N_2.

The *in-situ* DRIFT spectra of Pt-10CuO/$CeMnO_2$ catalyst, recorded under various reaction temperatures in an atmosphere of 60% H_2, 1% CO, 1% O_2, 20% CO_2, 3% H_2O, and balanced N_2, are presented in **Fig. 6a**. Three characteristic peaks appear on the catalysts: the characteristic peak located near 2020 cm^{-1} belonging to CO linear adsorption on Pt, the characteristic peak located at 2100 cm^{-1} belonging to CO adsorption on Cu^+ which has been considered as an effective site that can catalyze the CO-PROX reaction, and the characteristic peak located at 2171 cm^{-1} belonging to CO adsorption on Cu^{2+}, respectively[20, 24, 26, 63]. The characteristic peaks located at 2350 and 2310 cm^{-1} correspond to gas CO_2. As shown in Fig. 6a, the peak of CO linear adsorption on Pt basically does not change with the reaction temperature and only shows a slight red shift, which may be caused by the enhanced adsorption of CO on Pt with the rising temperatures[64]. The peak of CO adsorption on Cu^{2+} indicates that the catalyst is composed of both Cu^+ and Cu^{2+}, which is consistent with the results of XPS and H_2-TPR. It is noteworthy that the peak intensity of CO adsorption on Cu^+ sites gradually decreases with increasing reaction temperature, indicating that Cu^+ can efficiently catalyze the CO-PROX reaction to proceed at a lower temperature (80–140 °C) compared to Pt. This also coincides with the reduction of the high activity temperature range of the catalyst after the introduction of CuO, and indicates that the introduction of CuO provides additional Cu^+ sites for CO adsorption to the catalyst. The amount of CO adsorbed on each active site is shown in Fig. 6b. When both Cu and Pt sites available for CO adsorption are present on the catalyst, the total amount of CO adsorbed obtained the highest value in the temperature interval of 130–190 °C, which is favorable for the CO-PROX reaction. In summary, the introduction of Cu provided Cu^+ sites available for CO adsorption at low temperatures to compensate for the disadvantage of Pt catalysts at low temperatures, and the complete removal of CO at 130–190 °C was successfully achieved.

4 Conclusions

In conclusion, a series of Pt-CuO/$CeMnO_2$ catalysts have been effectively synthesized through a modified incipient-wetness impregnation and co-precipitation approach for CO-PROX reaction in practical conditions. The incorporation of CuO has been observed to enhance CO conversion and significantly elevate the performance of the preferential oxidation of CO in the presence of CO_2 and H_2O within a realistic application temperature window. Among them, the catalyst Pt-10CuO/$CeMnO_2$ was capable of achieving total CO oxidation within the temperature span of 130–190 °C, even in the presence of substantial quantities of CO_2 and H_2O in the feedstock. Remarkably, this catalytic performance endured over a period of 76 h without decline. Such an excellent catalytic performance can be attributed to the following aspects: (a) The part of CuO doped into the lattice of CeO_2 strongly interacts with Ce and generates a redox cycle ($Cu^{2+} + Ce^{3+} \rightarrow Cu^+ + Ce^{4+}$) that enhances the oxygen transfer capacity of the catalyst. (b) The part of CuO species on catalyst surface provides a large number of Cu^+ sites available for CO adsorption at low temperatures. This synergistic interaction with CO adsorbed on Pt sites ensures the selective and efficient conversion of CO across a broad temperature range, thereby meeting the demands of practical industrial conditions with the presence of CO_2 and H_2O. This work will provide a new approach to the design of low-cost, wide-temperature-range, and high-activity CO-PROX catalysts for practical application conditions.

References

[1] Li, J.; Zhu, P. F.; Zuo, S. F.; Huang, Q. Q.; Zhou, R. X. Influence of Mn doping on the performance of CuO-CeO_2 catalysts for selective oxidation of CO in hydrogen-rich streams. *Appl. Catal. A: Gen.* **2010**, *381*, 261–266.

[2] Lade, H.; Kumar, V.; Arthanareeswaran, G.; Ismail, A. F. Sulfonated poly(arylene ether sulfone) nanocomposite electrolyte membrane for fuel cell applications: A review. *Int. J. Hydrogen Energy* **2017**, *42*, 1063–1074.

[3] Wang, B. J.; Chu, G. W.; Li, Y. B.; Duan, X. Z.; Wang, J. X.; Luo, Y. Intensified micro-mixing effects on evolution of oxygen vacancies of CeO_2-based catalysts for improved CO oxidation. *Chem. Eng. Sci.* **2021**, *244*, 116814.

[4] Ren, P. C.; Tu, W. F.; Wang, C. C.; Cheng, S. F.; Liu, W. Q.; Zhang, Z. Z.; Tian, Y.; Han, Y. F. Mechanism and sites requirement for CO hydrogenation to CH_3OH over Cu/CeO_2 catalysts. *Appl. Catal. B: Environ.* **2022**, *305*, 121016.

[5] Ayastuy, J. L.; Gamboa, N. K.; González-Marcos, M. P.; Gutiérrez-Ortiz, M. A. CuO/CeO_2 washcoated ceramic monoliths for CO-PROX reaction. *Chem. Eng. J.* **2011**, *171*, 224–231.

[6] Wang, H. L.; Bootharaju, M. S.; Kim, J. H.; Wang, Y.; Wang, K.; Zhao, M.; Zhang, R.; Xu, J.; Hyeon, T.; Wang, X. et al. Synergistic interactions of neighboring platinum and iron atoms enhance reverse water–gas shift reaction performance. *J. Am. Chem. Soc.* **2023**, *145*, 2264–2270.

[7] Jia, Z. M.; Qin, X. T.; Chen, Y. L.; Cai, X. B.; Gao, Z. R.; Peng, M.; Huang, F.; Xiao, D. Q.; Wen, X. D.; Wang, N. et al. Fully-exposed Pt-Fe cluster for efficient preferential oxidation of CO towards hydrogen purification. *Nat. Commun.* **2022**, *13*, 6798.

[8] Snytnikov, P. V.; Zyryanova, M. M.; Sobyanin, V. A. CO-cleanup of hydrogen-rich stream for LT PEM FC feeding: Catalysts and their performance in selective CO methanation. *Top. Catal.* **2016**, *59*, 1394–1412.

[9] Gottesfeld, S.; Pafford, J. A new approach to the problem of carbon monoxide poisoning in fuel cells operating at low temperatures. *J. Electrochem. Soc.* **1988**, *135*, 2651–2652.

[10] Takenaka, S.; Shimizu, T.; Otsuka, K. Complete removal of carbon monoxide in hydrogen-rich gas stream through methanation over supported metal catalysts. *Int. J. Hydrogen Energy* **2004**, *29*, 1065–1073.

[11] Qiao, B. T.; Liang, J. X.; Wang, A. Q.; Liu, J. Y.; Zhang, T. Single atom gold catalysts for low-temperature CO oxidation. *Chin. J. Catal.* **2016**, *37*, 1580–1586.

[12] Qiao, B. T.; Liang, J. X.; Wang, A. Q.; Xu, C. Q.; Li, J.; Zhang, T.; Liu, J. J. Ultrastable single-atom gold catalysts with strong covalent metal-support interaction (CMSI). *Nano Res.* **2015**, *8*, 2913–2924.

[13] Komatsu, T.; Takasaki, M.; Ozawa, K.; Furukawa, S.; Muramatsu, A. PtCu intermetallic compound supported on alumina active for preferential oxidation of CO in hydrogen. *J. Phys. Chem. C.* **2013**, *117*, 10483–10491.

[14] Liu, K.; Wang, A. Q.; Zhang, T. Recent advances in preferential oxidation of CO reaction over platinum group metal catalysts. *ACS Catal.* **2012**, *2*, 1165–1178.

[15] Lu, J. C.; Wang, J.; Zou, Q.; He, D. D.; Zhang, L. M.; Xu, Z. Z.; He, S. F.; Luo, Y. M. Unravelling the nature of the active species as well as the doping effect over Cu/Ce-based catalyst for carbon monoxide preferential oxidation. *ACS Catal.* **2019**, *9*, 2177–2195.

[16] Fu, Q.; Li, W. X.; Yao, Y. X.; Liu, H. Y.; Su, H. Y.; Ma, D.; Gu, X. K.; Chen, L. M.; Wang, Z.; Zhang, H. et al. Interface-confined ferrous centers for catalytic oxidation. *Science* **2010**, *328*, 1141–1144.

[17] Dreyer, J. A. H.; Grossmann, H. K.; Chen, J. F.; Grieb, T.; Gong, B. B.; Sit, P. H. L.; Mädler, L.; Teoh, W. Y. Preferential oxidation of carbon monoxide over Pt-FeO_x/CeO_2 synthesized by two-nozzle flame spray pyrolysis. *J. Catal.* **2015**, *329*, 248–261.

[18] Davó-Quiñonero, A.; Bailón-García, E.; López-Rodríguez, S.; Juan-Juan, J.; Lozano-Castelló, D.; García-Melchor, M.; Herrera, F. C.;

Pellegrin, E.; Escudero, C.; Bueno-López, A. Insights into the oxygen vacancy filling mechanism in CuO/CeO_2 catalysts: A key step toward high selectivity in preferential CO oxidation. *ACS Catal.* **2020**, *10*, 6532–6545.

[19] Wang, B. B.; Zhang, H.; Xu, W.; Li, X. B.; Wang, W.; Zhang, L. J.; Li, Y. M.; Peng, Z.; Yang, F.; Liu, Z. Nature of active sites on Cu-CeO_2 catalysts activated by high-temperature thermal aging. *ACS Catal.* **2020**, *10*, 12385–12392.

[20] Jin, H.; You, R.; Zhou, S.; Ma, K.; Meng, M.; Zheng, L. R.; Zhang, J.; Hu, T. D. *In-situ* DRIFTS and XANES identification of copper species in the ternary composite oxide catalysts CuMnCeO during CO preferential oxidation. *Int. J. Hydrogen Energy* **2015**, *40*, 3919–3931.

[21] Wang, C. L.; Gu, X. K.; Yan, H.; Lin, Y.; Li, J. J.; Liu, D. D.; Li, W. X.; Lu, J. L. Water-mediated Mars–van Krevelen mechanism for CO oxidation on ceria-supported single-atom Pt_1 catalyst. *ACS Catal.* **2017**, *7*, 887–891.

[22] Wang, Y. R.; Ma, J. M.; Wang, X. Y.; Zhang, Z. S.; Zhao, J. H.; Yan, J.; Du, Y. P.; Zhang, H. B.; Ma, D. Complete CO oxidation by O_2 and H_2O over Pt-$CeO_{2-\delta}$/MgO following Langmuir–Hinshelwood and Mars–van Krevelen mechanisms, respectively. *ACS Catal.* **2021**, *11*, 11820–11830.

[23] Reina, T. R.; Papadopoulou, E.; Palma, S.; Ivanova, S.; Centeno, M. A.; Ioannides, T.; Odriozola, J. A. Could an efficient WGS catalyst be useful in the CO-PrO_x reaction. *Appl. Catal. B: Environ.* **2014**, *150–151*, 554–563.

[24] Davó-Quiñonero, A.; Navlani-García, M.; Lozano-Castelló, D.; Bueno-López, A.; Anderson, J. A. Role of hydroxyl groups in the preferential oxidation of CO over copper oxide-cerium oxide catalysts. *ACS Catal.* **2016**, *6*, 1723–1731.

[25] Hočevar, S.; Krašovec, U. O.; Orel, B.; Aricó, A. S.; Kim, H. CWO of phenol on two differently prepared CuO-CeO_2 catalysts. *Appl. Catal. B: Environ.* **2000**, *28*, 113–125.

[26] Gamarra, D.; Belver, C.; Fernández-García, M.; Martínez-Arias, A. Selective CO oxidation in excess H_2 over copper-ceria catalysts: Identification of active entities/species. *J. Am. Chem. Soc.* **2007**, *129*, 12064–12065.

[27] Teschner, D.; Wootsch, A.; Pozdnyakova-Tellinger, O.; Kröhnert, J.; Vass, E. M.; Hävecker, M.; Zafeiratos, S.; Schnörch, P.; Jentoft, F. C.; Knop-Gericke, A. Partial pressure dependent *in situ* spectroscopic study on the preferential CO oxidation in hydrogen (PROX) over Pt/ceria catalysts. *J. Catal.* **2017**, *249*, 318–327.

[28] Cao, J. L.; Zhang, X. Q.; Ou, X. X.; Liu, T.; Xing, T.; Li, Z.; Zhou, X.; Yan, H.; Liu, Y. B.; Feng, X. et al. Reactant adsorption modulation by Fe and K in Pt catalyst for highly effective CO preferential oxidation in practical conditions. *Chem. Eng. J.* **2022**, *444*, 136661.

[29] Huang, Y. Q.; Wang, A. Q.; Li, L.; Wang, X. D.; Su, D. S.; Zhang, T. "Ir-in-ceria": A highly selective catalyst for preferential CO oxidation. *J. Catal.* **2008**, *255*, 144–152.

[30] Yan, H.; Zhang, N. Q.; Wang, D. S. Highly efficient CeO_2-supported noble-metal catalysts: From single atoms to nanoclusters. *Chem Catalysis* **2022**.

[31] Naren, T.; Jing, G. J.; Xue, L.; Wang, Q.; Zhao, Y. S.; Li, C. X.; Lu, S. H.; Wu, J. F.; Zeng, S. H. Development of platinum assisted ternary catalyst with high activity and selectivity at working temperature of proton-exchange membrane fuel cells for preferential oxidation of CO. *Int. J. Hydrogen Energy* **2020**, *45*, 21848–21857.

[32] Wang, Q.; Gong, J. H.; Zhang, H.; Fan, Q. Y.; Xue, L.; Wu, J. F.; Li, J. X.; Wang, Y.; Liu, Z.; Gao, R. et al. Co-promotion of two-type active sites: PtCu single-atom alloy and copper-ceria interface for preferential oxidation of CO. *Appl. Catal. B: Environ.* **2022**, *306*, 121117.

[33] Maciel, C. G.; Silva, T. D. F.; Profeti, L. P. R.; Assaf, E. M.; Assaf, J. M. Study of CuO/CeO_2 catalyst with for preferential CO oxidation reaction in hydrogen-rich feed (PROX-CO). *Appl. Catal. A: Gen.* **2012**, *431–432*, 25–32.

[34] Meng, M.; Tu, Y. B.; Ding, T.; Sun, Z. S.; Zhang, L. J. Effect of synthesis pH and Au loading on the CO preferential oxidation performance of Au/MnO_x-CeO_2 catalysts prepared with ultrasonic assistance. *Int. J. Hydrogen Energy* **2011**, *36*, 9139–9150.

[35] He, C.; Yu, Y. K.; Shen, Q.; Chen, J. S.; Qiao, N. L. Catalytic behavior and synergistic effect of nanostructured mesoporous CuO-MnO_x-CeO_2 catalysts for chlorobenzene destruction. *Appl. Surf. Sci.* **2014**, *297*, 59–69.

[36] Kim, H. J.; Jang, M. G.; Shin, D.; Han, J. W. Design of ceria catalysts for low-temperature CO oxidation. *ChemCatChem* **2020**, *12*, 11–26.

[37] Miranda Cruz, A. R.; Assaf, E. M.; Gomes, J. F.; Assaf, J. M. New insights about the effect of the synthesis method on the CuO CeO_2 redox properties and catalytic performance towards CO-PROX reaction for fuel cell applications. *J. Environ. Manage.* **2019**, *242*, 272–278.

[38] Tiscornia, I. S.; Lacoste, A. M.; Gómez, L. E.; Boix, A. V. CuO-CeO_2/SiO_2 coating on ceramic monolith: Effect of the nature of the catalyst support on CO preferential oxidation in a H_2-rich stream. *Int. J. Hydrogen Energy* **2022**, *45*, 6636–6650.

[39] Zhang, H.; Zhao, X. Z.; Wang, S.; Zeng, S. H.; Su, H. Q. Change of Cu^+ species and synergistic effect of copper and cerium during reduction–oxidation treatment for preferential CO oxidation. *Appl. Surf. Sci.* **2018**, *441*, 754–763.

[40] Gao, Y. X.; Xie, K. M.; Wang, W. D.; Mi, S. Y.; Liu, N.; Pan, G. Q.; Huang, W. X. Structural features and catalytic performance in CO preferential oxidation of CuO-CeO_2 supported on multi-walled carbon nanotubes. *Catal. Sci. Technol.* **2015**, *5*, 1568–1579.

[41] Zou, Q.; Zhao, Y. H.; Jin, X.; Fang, J.; Li, D. Y.; Li, K. Z.; Lu, J. C.; Luo, Y. M. Ceria-nano supported copper oxide catalysts for CO preferential oxidation: Importance of oxygen species and metal–support interaction. *Appl. Surf. Sci.* **2019**, *494*, 1166–1176.

[42] Guo, X. L.; Qiu, Z. H.; Mao, J. X.; Zhou, R. X. Shape-controlled $Cu_xCe_{1-x}O_2$ nanorods catalyst and the active components functioned in selective oxidation of CO in hydrogen-rich stream. *J. Power Sources* **2020**, *451*, 227757.

[43] Ayastuy, J. L.; Fernández-Puertas, E.; González-Marcos, M. P.; Gutiérrez-Ortiz, M. A. Transition metal promoters in CuO/CeO_2 catalysts for CO removal from hydrogen streams. *Int. J. Hydrogen Energy* **2012**, *37*, 7385–7397.

[44] Fan, J.; Wu, X. D.; Wu, X. D.; Liang, Q.; Ran, R.; Weng, D. Thermal ageing of Pt on low-surface-area CeO_2-ZrO_2-La_2O_3 mixed oxides: Effect on the OSC performance. *Appl. Catal. B: Environ.* **2008**, *81*, 38–48.

[45] Xie, Y.; Wu, J. F.; Jing, G. J.; Zhang, H.; Zeng, S. H.; Tian, X. P.; Zou, X.; Wen, J.; Su, H. Q.; Zhong, C. J. et al. Structural origin of high catalytic activity for preferential CO oxidation over CuO/CeO_2 nanocatalysts with different shapes. *Appl. Catal. B: Environ.* **2018**, *239*, 665–676.

[46] Guo, X. L.; Li, J.; Zhou, R. X. Catalytic performance of manganese doped CuO-CeO_2 catalysts for selective oxidation of CO in hydrogen-rich gas. *Fuel* **2016**, *163*, 56–64.

[47] Qi, L.; Yu, Q.; Dai, Y.; Tang, C. J.; Liu, L. J.; Zhang, H. L.; Gao, F.; Dong, L.; Chen, Y. Influence of cerium precursors on the structure and reducibility of mesoporous CuO-CeO_2 catalysts for CO oxidation. *Appl. Catal. B: Environ.* **2012**, *119–120*, 308–320.

[48] Trovarelli, A.; Llorca, J. Ceria catalysts at nanoscale: How do crystal shapes shape catalysis. *ACS Catal.* **2017**, *7*, 4716–4735.

[49] Wang, C. X.; Feng, F.; Du, J. C.; Zheng, T. T.; Pan, Z. F.; Zhao, Y. K. Activation of surface lattice oxygen in ceria supported Pt/Al_2O_3 catalyst for low-temperature propane oxidation. *ChemCatChem* **2019**, *11*, 2054–2057.

[50] Zhang, S. R.; Shan, J. J.; Zhu, Y.; Frenkel, A. I.; Patlolla, A.; Huang, W. X.; Yoon, S. J.; Wang, L.; Yoshida, H.; Takeda, S. et al. WGS catalysis and *in situ* studies of CoO_{1-x}, $PtCo_n/Co_3O_4$, and $Pt_mCo_{m'}/CoO_{1-x}$ nanorod catalysts. *J. Am. Chem. Soc.* **2013**, *135*, 8283–8293.

[51] Jeong, H.; Shin, D.; Kim, B. S.; Bae, J.; Shin, S.; Choe, C.; Han, J. W.; Lee, H. Controlling the oxidation state of Pt single atoms for

maximizing catalytic activity. *Angew. Chem., Int. Ed.* **2020**, *59*, 20691–20696.

[52] Kundakovic, L.; Flytzani-Stephanopoulos, M. Reduction characteristics of copper oxide in cerium and zirconium oxide systems. *Appl. Catal. A: Gen.* **1998**, *171*, 13–29.

[53] Qiu, H. J.; Shen, X.; Wang, J. Q.; Hirata, A.; Fujita, T.; Wang, Y.; Chen, M. W. Aligned nanoporous Pt-Cu bimetallic microwires with high catalytic activity toward methanol electrooxidation. *ACS Catal.* **2015**, *5*, 3779–3785.

[54] Liu, X. H.; Wang, X. H.; Zhen, S. Y.; Sun, G. D.; Pei, C. L.; Zhao, J. J.; Gong, J. J. Support stabilized PtCu single-atom alloys for propane dehydrogenation. *Chem. Sci.* **2022**, *13*, 9537–9543.

[55] Wang, W. W.; Du, P. P.; Zou, S. H.; He, H. Y.; Wang, R. X.; Jin, Z.; Shi, S.; Huang, Y. Y.; Si, R.; Song, Q. S. Highly dispersed copper oxide clusters as active species in copper-ceria catalyst for preferential oxidation of carbon monoxide. *ACS Catal.* **2015**, *5*, 2088–2099.

[56] Kandoi, S.; Gokhale, A. A.; Grabow, L. C.; Dumesic, J. A.; Mavrikakis, M. Why Au and Cu are more selective than Pt for preferential oxidation of CO at low temperature. *Catal. Lett.* **2004**, *93*, 93–100.

[57] Zhuang, L. Z.; Ge, L.; Yang, Y. S.; Li, M. R.; Jia, Y.; Yao, X. D.; Zhu, Z. H. Ultrathin iron-cobalt oxide nanosheets with abundant oxygen vacancies for the oxygen evolution reaction. *Adv. Mater.* **2017**, *29*, 1606793.

[58] Wang, S.; Guan, B. Y.; Lou, X. W. Rationally designed hierarchical N-doped carbon@$NiCo_2O_4$ double-shelled nanoboxes for enhanced visible light CO_2 reduction. *Energy Environ. Sci.* **2018**, *11*, 306–310.

[59] Liu, Y.; Xue, W. C.; Liu, X. Q.; Wei, F.; Lin, X. H.; Lu, X. F.; Lin, W.; Hou, Y. D.; Zhang, G. G.; Wang, S. B. Ultrafine Pt nanoparticles on defective tungsten oxide for photocatalytic ethylene synthesis. *Small* **2024**, *20*, 2402004.

[60] Wei, F.; Xue, W. C.; Yu, Z. Y.; Lu, X. F.; Wang, S. B.; Lin, W.; Wang, X. C. Dynamic cooperations between lattice oxygen and oxygen vacancies for photocatalytic ethane dehydrogenation by a self-restoring $LaVO_4$ catalyst. *Chin. Chem. Lett.* **2024**, *35*, 171–176.

[61] Polster, C. S.; Nair, H.; Baertsch, C. D. Study of active sites and mechanism responsible for highly selective CO oxidation in H_2 rich atmospheres on a mixed Cu and Ce oxide catalyst. *J. Catal.* **2009**, *266*, 308–319.

[62] Li, J.; Zhu, P. F.; Zhou, R. X. Effect of the preparation method on the performance of CuO-MnO_x-CeO_2 catalysts for selective oxidation of CO in H_2-rich streams. *J. Power Sources* **2011**, *196*, 9590–9598.

[63] Yao, S. Y.; Mudiyanselage, K.; Xu, W. Q.; Johnston-Peck, A. C.; Hanson, J. C.; Wu, T. P.; Stacchiola, D.; Rodriguez, J. A.; Zhao, H. Y.; Beyer, K. A. et al. Unraveling the dynamic nature of a CuO/CeO_2 catalyst for CO oxidation in operando: A combined study of XANES (fluorescence) and DRIFTS. *ACS Catal.* **2014**, *4*, 1650–1661.

[64] Kaftan, A.; Kusche, M.; Laurin, M.; Wasserscheid, P.; Libuda, J. KOH-promoted Pt/Al_2O_3 catalysts for water gas shift and methanol steam reforming: An operando DRIFTS-MS study. *Appl. Catal. B: Environ.* **2017**, *201*, 169–181.

Data availability

All data required to support the conclusions of the paper are listed in the manuscript and the supplementary Information. Additional data related to this article are available from the corresponding author upon request.

Acknowledgements

This work was supported by the Distinguished Young Scholars of the National Natural Science Foundation of China (No. 22322814), the National Natural Science Foundation of China (Nos. 21978325 and 51876075), and the Science and Technology Innovation Project of the Shandong Energy Group Co., Ltd. (Nos. SNKJ2021BJ05-R05 and 9000B2024000030).

Author contributions

J. L. C.: investigation, validation, formal analysis, data curation; T. X.: investigation, writing—original draft, review and editing; Z. Z. S. and S. W.: formal analysis, data curation, and visualization; J. Q. W. and L. X. M.: validation; Z. L., T. X., Y. X. T., H. Y., Y. B. L., and C. H. Y.: supervision; X. Z.: supervision, writing-review & editing; X. F.: methodology, software, writing—review and editing; D. C.: conceptualization, project administration, supervision, funding acquisition, writing—review and editing.

Competing interests

The authors have no competing interests to declare that are relevant to this article.

Use of AI statement

None.

Additional information

Supplementary Information. The online version contains supplementary material available at https://doi.org/10.26599/CF.2025.9200038.